Interference in a Quantum Channel Due to Classical Four-Wave Mixing in Optical Fibers

Nuno A. Silva, Álvaro J. Almeida, and Armando N. Pinto, *Senior Member, IEEE*

***Abstract*— The second-order coherence function for idler photons generated through stimulated four-wave mixing (FWM) is theoretically derived, considering both spontaneous and stimulated Raman contributions. Two distinct cases and two different power regimes are analyzed. First, we consider that the idler wave is fully generated inside the fiber. In a second scenario, we admit that at the fiber input there exist a quantum channel and idler photons will be created at that frequency through the combined processes of FWM and Raman scattering. Results show that for the first case, in a low power regime, the idler photons follow a thermal statistics. In a moderate power regime, the statistics of the generated idler wave presents a Poissonian distribution. Results also show that in the second case, in a low power regime, the statistics of the input quantum channel goes from a Poissonian statistics at the fiber input to a thermal statistics at the fiber output. Findings show that in a moderate power regime, the quantum channel maintains its Poissonian distribution through fiber propagation.**

***Index Terms*— Nonlinear optics, nonlinearities, optical mixing, Raman scattering.**

I. Introduction

QUANTUM key distribution (QKD) systems have evolved from point-to-point fiber links to optical fiber networks. In that scenario, the quantum channel used in the QKD setup share the same fiber with other classical optical signals [1]. In that scenario, the inter-channel nonlinear effects that occurs inside the fiber can potentially degrade the performance of the QKD system [2]. In [3], the quantum channel and the classical signal shared the same fiber, but they were placed in different bands. However, there are important advantages in placing the QKD channel on the C-band, as fiber losses and most of the installed optical components are optimized for the C-band [4], [5]. Recently in [6], authors demonstrated that quantum channels can successfully coexist with classical optical signals in the same optical band, in a wavelength-division multiplexed (WDM) architecture [6]. In a WDM lightwave system, the interaction between the classical optical signals will generate noise photons through stimulated FWM and through spontaneous and stimulated Raman scattering [7], [8]. These physical impairments were investigated in recent works in this coexisting architecture [2], [8], [9]. The statistical characterization of the quantum channel is essential to correctly estimate the quantum bit error rate (QBER). Changes in the QBER are used in several QKD protocols to detect the presence of an eavesdropper [1]. However, the theoretical statistical characterization of the quantum channel in this coexisting architecture remains an open issue, to the best of our knowledge.

The experimental statistical characterization of an optical field can be performed with several different techniques [10]–[14]. A method based on quantum tomography was used in [10]. That particular method requires phase-matching with a local oscillator and homodyne detection. A different experiment approach to measure the statistics of an optical field was implemented in [11]. In that case, authors have used a photomultiplier tube to reconstruct the statistics of an incoming quantum state. In [12], authors reconstruct the photon statistics by using on/off detectors assisted by the maximum-likelihood estimation algorithm. Recently, the second-order coherence function, $g^{(2)}(0)$, was measured experimentally for a heralded single photon source based on the spontaneous FWM process inside an optical fiber [13]–[17]. The photon number statistics of the heralded single-photon source based on spontaneous FWM process was also studied in [18] through the Wigner function. Moreover, in [15] authors measured the unconditional second-order correlation function for the spontaneous FWM process inside a microstruture fiber. In [10], authors report measurements of the photon statistics of a fiber-optic parametric amplifier. In that experimental work, the idler wave is fully generated inside the fiber, and they measure the statistics of the signal field for a high gain fiber-optic parametric amplifier based on the FWM process.

The focus of this paper is to understand the impact of noise photons generated by FWM and Raman scattering on the statistics of a coherent quantum channel used for QKD. In this study, we admit that the spectral bandwidth of the noise photons coincide with the wavelength of the quantum channel. We quantify the photon statistics of the quantum channel by means of the second-order coherence function. We present a quantum description of the FWM process in optical fibers considering both stimulated and spontaneous Raman scattering. The photon number distribution of the idler wave generated through stimulated FWM is studied in two distinct cases. First, we assume that the idler photons are fully

Manuscript received July 25, 2011; revised December 7, 2011; accepted January 17, 2012. Date of publication January 23, 2012; date of current version February 14, 2012. This work was supported in part by the Fundação para a Ciência e Tecnologia (FCT) under Ph.D. Grant SFRH/BD/63958/2009 and Grant SFRH/BD/79482/2011, and in part by the FCT and European Union FEDER Program through the PTDC/EEA-TEL/103402/2008-QuantPrivTel Project and P-Quantum IT/LA Project.

N. A. Silva and A. N. Pinto are with the Department of Electronics, Telecommunications and Informatics, University of Aveiro and Instituto de Telecomunicações, Aveiro 3810-193, Portugal (e-mail: nasilva@av.it.pt; anp@ua.pt).

Á. J. Almeida is with the Department of Physics, University of Aveiro and Instituto de Telecomunicações, Aveiro 3810-193, Portugal (e-mail: aalmeida@av.it.pt).

Color versions of one or more of the figures in this paper are available online at http://ieeexplore.ieee.org.

Digital Object Identifier 10.1109/JQE.2012.2185219

generated inside the fiber. In a second scenario, we admit that at the fiber input there exists a coherent quantum signal and idler photons will be created at that frequency.

This paper contains five sections. In section II, we present a quantum version of the stimulated FWM process. In section III, we discuss the second-order coherence function for the stimulated FWM process. Section IV reports the theoretical results. The main conclusions of this paper are summarized in section V.

II. FWM Process

In this section, we present a quantum description of the generation of the idler wave through the FWM process inside an optical fiber. In Fig. 1, we present a schematic arrangement of a typical FWM experimental setup. We assume that all fields remain co-polarized along the propagation on the fiber, and the fiber attenuation is negligible. In that conditions, the quantum evolution of the idler annihilation operator in the frequency domain inside the optical fiber is given by the input/output relation [19], [20]

$$\hat{A}(L,\omega_i) = \Big(\Lambda_i(L)\hat{A}(0,\omega_Q) + \Gamma_i(L)e^{-2i\theta_p}\hat{A}^\dagger(0,\omega_s) + \hat{M}(L,\omega_i)\Big)\Theta(L) \tag{1}$$

where θ_p is the phase of the optical pump coherent field, ω_Q is the frequency of the input quantum channel, ω_i is the frequency of the idler photons generated through FWM process and Raman scattering inside the fiber, which we assume coincident with ω_Q. In (1), $\Theta(L) = \exp\{i(k_p + \gamma P_p)L\}$, where k_p is the pump propagation constant, P_p is the fiber input pump power, γ is the fiber nonlinear parameter, L is the fiber length. In (1)

$$\Lambda_i(L) = \left(\cosh(g_{ip}L) + i\frac{\kappa_{ip}}{2g_{ip}}\sinh(g_{ip}L)\right)e^{i\frac{k_i-k_s}{2}L}, \tag{2}$$

$$\Gamma_i(L) = i\frac{\gamma\,\eta_{ip}}{g_{ip}}A_p^2\sinh(g_{ip}L)e^{i\frac{k_i-k_s}{2}L} \tag{3}$$

and

$$\hat{M}(L,\omega_i) = i\int_0^L \hat{m}_{ip}(z)\Big(A_p e^{-i\theta_p}\Lambda_i(L-z) - A_p^* e^{i\theta_p}\Gamma_i(L-z)\Big)dz \tag{4}$$

where $\hat{m}_{ip}(z)$ is the Hermitian phase noise operator, and A_p is the pump field envelop such that $P_p = |A_p|^2$. In (2)-(4)

$$g_{ip}^2 = \left((\gamma\,\eta_{ip}P_p)^2 - (\kappa_{ip}/2)^2\right), \tag{5a}$$

$$\kappa_{ip} = \Delta\beta + 2\gamma\,P_p\eta_{ip}\,, \tag{5b}$$

$$\eta_{ip} = 1 - f_R + f_R\left(\tilde{R}_a(\omega_i-\omega_p) + \tilde{R}_b(\omega_i-\omega_p)\right) \tag{5c}$$

where $\Delta\beta$ is the phase-matching condition given by [21]

$$\Delta\beta \approx \beta_3(\omega_p-\omega_0)(\omega_p-\omega_s)^2 + \frac{\beta_4}{2}\left[(\omega_p-\omega_0)^2 + \frac{1}{6}(\omega_p-\omega_s)^2\right](\omega_p-\omega_s)^2 \tag{6}$$

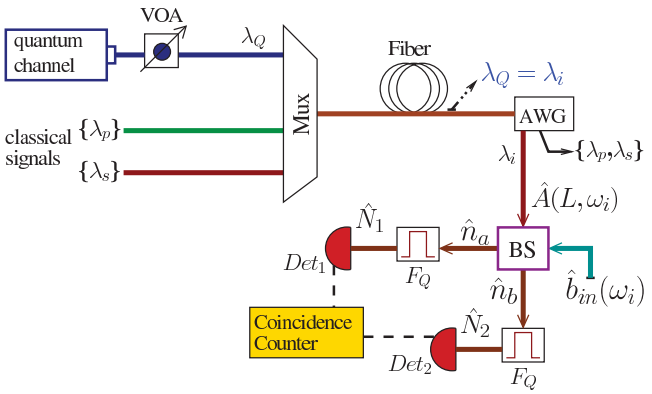

Fig. 1. Setup for obtain the photon counting statistics of the stimulated FWM process. The dashed lines represent electrical signals and the solid lines the optical path. Details of the setup are presented in the text.

where ω_p and ω_s are the pump and signal frequencies, respectively, ω_0 is fiber zero-dispersion frequency, and β_3 and β_4 are the third and fourth order dispersion coefficients, respectively. In (5), $f_R = 0.245$ is the fractional contribution of the Raman process to the nonlinear refractive index, $\tilde{R}_a(\omega_i-\omega_p)$ and $\tilde{R}_b(\omega_i-\omega_p)$ are the isotropic and anisotropic Raman response, respectively, defined in [7], [22]–[24]. In (1), the field operator satisfies the commutation relation [19]

$$\left[\hat{A}(0,\omega_u), \hat{A}^\dagger(0,\omega_u')\right] = 2\pi\,\delta(\omega_u-\omega_u') \tag{7}$$

where $u = s$ or Q, and the noise quantum operator [19], [25]

$$\left[\hat{M}(L,\omega_i), \hat{M}^\dagger(L,\omega_i')\right] = 2\pi\left(|\Lambda_i(L)|^2 - |\Gamma_i(L)|^2 - 1\right)\delta(\omega_i-\omega_i'). \tag{8}$$

The photon number distribution of the idler wave can be obtained through the setup shown in Fig. 1 [13], [26]. In Fig. 1, a pump, λ_p, a classical signal λ_s, and a quantum channel λ_Q are multiplexed by a Mux and sent to an optical fiber. The quantum channel λ_Q is highly attenuated with a variable optical attenuator (VOA). Note that if the idler wave is fully generated inside the fiber, the quantum channel path present in Fig. 1 does not exist. Inside the fiber idler photons are created due to the both stimulated and spontaneous FWM and Raman scattering processes. Since we assume that the idler photons have wavelength $\lambda_i = \lambda_Q$, noise photons will be added to the quantum channel launched to the fiber. At the fiber output, the three optical fields passes through an arrayed waveguide grating (AWG) to separate the pump and signal fields from the quantum channel λ_Q. The output photons from the AWG are launched into a non-polarizing beam splitter (BS), where they can be combined with other quantum states given by the $\hat{b}_{in}(\omega)$ operator. At the beam splitter output the photons are spectrally filtered (F_Q) and collected by the photon counting modules, Det_1 and Det_2. Single and coincidence measurements are performed in order to obtain $g^{(2)}(0)$ [14].

A. Expectation Values

We are now interested on the evaluation of the expectation values for the photon flux spectral density and the normally

ordered second moment, for the idler photons generated through FWM and Raman scattering processes. We take at the input of the fiber the signal field and the quantum channel as a continuous mode coherent state, as well states $|f\rangle$ that accounts the phonon reservoir inside the fiber. The general state can be written as [13], [25], [27]

$$|\Psi\rangle = \exp\left\{\int d\omega_s \left(\vartheta(\omega_s)\hat{A}^\dagger(0,\omega_s) - c.c.\right)\right\}|0_s\rangle \times \exp\left\{\int d\omega_Q \left(\varphi(\omega_Q)\hat{A}^\dagger(0,\omega_Q) - c.c.\right)\right\}|0_Q\rangle \tag{9}$$

where $c.c.$ represents the complex conjugate, $|0_u\rangle$ is the vacuum state for the $u = s$ or Q mode, $\vartheta(\omega_s)$ and $\varphi(\omega_Q)$ are the fiber incident amplitudes for the fields $\hat{A}(0,\omega_s)$ and $\hat{A}(0,\omega_Q)$, respectively. That amplitudes contain the mean photon flux and the phase of the optical field.

The expectation values for the noise operator $\hat{M}(L,\omega_i)$ are given by [25]

$$\langle f|\hat{M}^\dagger(L,\omega_i)|f\rangle = \langle f|\hat{M}(L,\omega_i)|f\rangle = 0, \tag{10a}$$

$$\langle f|\hat{M}(L,\omega_i)\hat{M}(L,\omega_i')|f\rangle = \langle f|\hat{M}^\dagger(L,\omega_i)\hat{M}^\dagger(L,\omega_i')|f\rangle = 0 \tag{10b}$$

and

$$\langle f|\hat{M}^\dagger(L,\omega_i)\hat{M}(L,\omega_i')|f\rangle = 2\pi\left(n_{th}(\omega_i-\omega_p)+1\right) \times \left(|\Lambda_i(L)|^2 - |\Gamma_i(L)|^2 - 1\right) \delta(\omega_i-\omega_i') \tag{11}$$

where $n_{th}(\Omega) = \left[e^{\hbar|\Omega|/k_BT} - 1\right]^{-1}$. The fourth-order noise correlation function of the noise operator used for obtain the normally ordered second moment is expressed in terms of second-order correlation [25]

$$\begin{aligned}&\langle f|\hat{M}^\dagger(L,\omega_i)\hat{M}^\dagger(L,\omega_i')\hat{M}(L,\omega_i'')\hat{M}(L,\omega_i''')|f\rangle \\ &= \langle f|\hat{M}^\dagger(L,\omega_i)\hat{M}(L,\omega_i'')|f\rangle\langle f|\hat{M}^\dagger(L,\omega_i')\hat{M}(L,\omega_i''')|f\rangle \\ &+ \langle f|\hat{M}^\dagger(L,\omega_i)\hat{M}(L,\omega_i''')|f\rangle\langle f|\hat{M}^\dagger(L,\omega_i') \\ &\times \hat{M}(L,\omega_i'')|f\rangle\end{aligned} \tag{12}$$

and each expectation noise value is evaluated using (11).

The expectation value for the signal quantum operator is given by [28]–[30]

$$\begin{aligned}&\langle\Psi\left|\left(\hat{A}^\dagger(0,\omega_s')\right)^m\left(\hat{A}(0,\omega_s'')\right)^n\right|\Psi\rangle \\ &= \left(\langle\Psi|\hat{A}^\dagger(0,\omega_s')|\Psi\rangle\right)^m\left(\langle\Psi|\hat{A}(0,\omega_s'')|\Psi\rangle\right)^n \\ &= \left(\vartheta^*(\omega_s')\right)^m\left(\vartheta(\omega_s'')\right)^n.\end{aligned} \tag{13}$$

A similiar expression is obtained for the input coherent quantum channel ω_Q. Although (13) is null if $\vartheta(\omega_s) = 0$, idler photons are generated inside the fiber due to the fact that, the anti-normal ordered moments that arises from (1) are not null even when $\vartheta(\omega_s) = 0$.

B. Beam Splitter Input/Output Relations

The second-order coherence parameter can be experimentally obtained with one non-polarizing beam splitter [14], [15] through the setup shown in Fig. 1. In that setup, we consider that the arm $\hat{b}_{in}$ of the beam splitter is left in its vacuum state given by $|0_b\rangle$. In reality beam splitters exhibit some losses. This mean that some of the incident idler photons are absorbed by the beam splitter. In Fig. 1, $\hat{n}_a = \hat{a}_{out}^\dagger(\omega_i)\hat{a}_{out}(\omega_i)$ and $\hat{n}_b = \hat{b}_{out}^\dagger(\omega_i)\hat{b}_{out}(\omega_i)$ where [31]

$$\hat{a}_{out}(\omega_i) = t(\omega_i)\hat{A}(L,\omega_i) + r(\omega_i)\hat{b}_{in}(\omega_i) + \hat{F}_a(\omega_i), \tag{14}$$

$$\hat{b}_{out}(\omega_i) = t(\omega_i)\hat{b}_{in}(\omega_i) + r(\omega_i)\hat{A}(L,\omega_i) + \hat{F}_b(\omega_i) \tag{15}$$

where $r(\omega_i)$ and $t(\omega_i)$ are the beam splitter reflection and transmission coefficients, respectively, and $\hat{F}_v(\omega_i)$ is the Langevin noise operator, with $v = a, b$, which satisfy the commutation relations [31]

$$\left[\hat{F}_v(\omega_i), \hat{F}_v^\dagger(\omega_i')\right] = 2\pi\left(1 - |t_i|^2 - |r_i|^2\right)\delta(\omega_i-\omega_i') \tag{16a}$$

$$\left[\hat{F}_v(\omega_i), \hat{F}_l^\dagger(\omega_i')\right] = -2\pi\left(t_i r_i^* + r_i t_i^*\right)\delta(\omega_i-\omega_i') \tag{16b}$$

with $l \neq v = a, b$. The expectation values for the Langevin noise operators are [31]

$$\langle\hat{F}_v(\omega_i)\rangle = \langle\hat{F}_v^\dagger(\omega_i)\rangle = 0, \tag{17a}$$

$$\langle\hat{F}_v(\omega_i)\hat{F}_v^\dagger(\omega_i')\rangle = 2\pi\left(1 - |t_i|^2 - |r_i|^2\right)\delta(\omega_i-\omega_i') \tag{17b}$$

$$\langle\hat{F}_v(\omega_i)\hat{F}_l^\dagger(\omega_i')\rangle = -2\pi\left(t_i r_i^* + r_i t_i^*\right)\delta(\omega_i-\omega_i') \tag{17c}$$

where $t_i = t(\omega_i)$ and $r_i = r(\omega_i)$.

III. Photon Number Distribution

In this section, we examine the photon counting statistics of the idler wave fully generated inside the fiber, and how the idler photons generated through FWM and Raman scattering processes affects the photon number distribution of an incident coherent quantum channel. The photon number distribution is studied theoretically in terms of the second-order coherence function, $g^{(2)}(0)$. The second-order coherence function is defined as [13]

$$g^{(2)}(0) = \frac{\langle : \hat{N}_1\hat{N}_2 : \rangle}{\langle\hat{N}_1\rangle\langle\hat{N}_2\rangle}, \tag{18}$$

where $\hat{N}_1$ and $\hat{N}_2$ are the photon number operators, according with Fig. 1, and :: denotes operator normal ordering. A vanishing $g^{(2)}(0)$ corresponds to a perfect single photon source, while $g^{(2)}(0) < 1$ determines the nonclassical nature of the optical field. Otherwise, $g^{(2)}(0) \geq 1$ represents the classical nature of the field being measured. In addition, it can be shown that $g^{(2)}(0) = 1$ corresponds to a Poissonian statistics, such as a coherent laser, and $g^{(2)}(0) = 2$ determines a source with thermal statistics, such as spontaneous Raman scattering [13], [15], [17].

As seen in Fig. 1 after the beam splitter the optical field is filtered using an optical filter to remove outband photons,

mainly from the pump and signal fields. In that case, the filtered idler field in time domain can be written as [19], [25]

$$\hat{a}_i(t) = \frac{1}{2\pi}\int d\omega_i H(\omega_i)\hat{a}_{out}(\omega_i)e^{-i\omega_i t}, \tag{19}$$

$$\hat{b}_i(t) = \frac{1}{2\pi}\int d\omega_i H(\omega_i)\hat{b}_{out}(\omega_i)e^{-i\omega_i t} \tag{20}$$

where $H(\omega_i)$ is the filter function centered in $\bar{\omega}_i$ and angular frequency bandwidth $\sigma_{\bar{\omega}_i} = 2\pi(\Delta\nu_{\bar{\omega}_i})$. We assume that $g^{(2)}(0)$ is measured by direct photodetection, and there is no background noise at the detection stage. Note that in a direct detection configuration the background noise does not affect the value of $g^{(2)}(0)$, for a detected coherent optical field [32], [33]. For a thermal field the background noise slightly decrease the $g^{(2)}(0)$ parameter [32], [33]. Assuming ideal detection, the expectation value for the dimensionless number operator is given by [25]

$$\begin{aligned}\langle\hat{N}_n\rangle &= \int_{t_0}^{t_0+T_0} dt\langle\hat{c}_i^{\dagger}(t)\hat{c}_i(t)\rangle \\ &= \frac{1}{(2\pi)^2}\int_{t_0}^{t_0+T_0} dt\int d\omega_i'\int d\omega_i'' H^*(\omega_i')H(\omega_i'') \\ &\quad\times\langle\hat{c}_{out}^{\dagger}(\omega_i')\hat{c}_{out}(\omega_i'')\rangle e^{i(\omega_i'-\omega_i'')t}\end{aligned} \tag{21}$$

where $\hat{c} = \hat{a}$ for $n = 1$ and $\hat{c} = \hat{b}$ for $n = 2$. In Fig. 1, $n = 1$ corresponds to Det_1, whereas $n = 2$ corresponds to Det_2. The normally ordered second moment can be written as [25]

$$\begin{aligned}\langle :\hat{N}_1\hat{N}_2: \rangle &= \frac{1}{(2\pi)^4}\int_{t_0}^{t_0+T_0} dt\int_{t_0}^{t_0+T_0} dt'\int d\omega_i'\int d\omega_i'' \\ &\quad\times\int d\omega_i'''\int d\omega_i'''' \\ &\quad\times H^*(\omega_i')H^*(\omega_i'')H(\omega_i''')H(\omega_i'''') \\ &\quad\times\langle\hat{a}_{out}^{\dagger}(\omega_i')b_{out}^{\dagger}(\omega_i'')\hat{b}_{out}(\omega_i''')\hat{a}_{out}(\omega_i'''')\rangle \\ &\quad\times e^{i(\omega_i'-\omega_i'''')t}e^{i(\omega_i''-\omega_i''')t'}\end{aligned} \tag{22}$$

where $t_0 + T_0$ is a period of time in which the photocurrent of the direct detection measurements is integrated.

In this work, we admit that all fields sent to the fiber are from different lasers, in which only a single mode is excited. In that case

$$\vartheta(\omega_s) = (2\pi I_s)^{1/2} e^{-i\theta_s}\delta(\omega_Q - \bar{\omega}_Q), \tag{23a}$$

$$\varphi(\omega_Q) = \left(2\pi I_Q\right)^{1/2} e^{-i\theta_Q}\delta(\omega_Q - \bar{\omega}_Q) \tag{23b}$$

where $\omega_s = 2\omega_p - \omega_Q$, $\bar{\omega}_Q$ is the laser excited mode, which coincides with the filter central frequency $\bar{\omega}_i$. In (23), I_s and I_Q are the signal field and coherent quantum channel input mean photon flux, given by

$$I_u = P_u/(\hbar\omega_u). \tag{24}$$

If we assume that $\sigma_{\bar{\omega}_i} \ll \omega_i$ and $\sigma_{\bar{\omega}_i}T_0 \ll 1$ the multiple integrals in (21) and (22) can be carried out

$$\begin{aligned}\langle\hat{N}_n\rangle \simeq \left(T_0\Delta\nu_{\bar{\omega}_i}\right)|X_i|^2\Big(&\bar{n}_Q|\Lambda_i|^2 + (1+\bar{n}_s)|\Gamma_i|^2 \\ &+ (\bar{n}_{th}+1)\left(|\Lambda_i|^2 - |\Gamma_i|^2 - 1\right) \\ &+ 2\text{Re}\Big[\Lambda_i\Gamma_i^* e^{-i\Delta\theta}\Big](\bar{n}_Q\bar{n}_s)^{1/2}\Big),\end{aligned} \tag{25}$$

where the number operator was obtained from the state given by (9), $X_i = t(\bar{\omega}_i)$ for $n = 1$ and $X_i = r(\bar{\omega}_i)$ for $n = 2$, and $\Delta\nu_{\bar{\omega}_i} = (1/2\pi)\int|H(\omega_i)|^2 d\omega_i$. In (25), $\bar{n}_Q$ and $\bar{n}_s$ are the fiber input mean photon fluxes per unit of angular frequency bandwidth $\sigma_{\bar{\omega}_i}$. Finally, the normally ordered second moment is given by

$$\begin{aligned}\langle :\hat{N}_1\hat{N}_2: \rangle \simeq \left(T_0\Delta\nu_{\bar{\omega}_i}\right)^2|\bar{r}_i|^2|\bar{t}_i|^2\Big(&\bar{n}_Q^2|\Lambda_i|^4 \\ &+4\bar{n}_Q(1+\bar{n}_s)|\Lambda_i|^2|\Gamma_i|^2 + 2\bar{n}_Q\bar{n}_s\text{Re}\Big[\Lambda_i^2\Gamma_i^{*2}e^{-2i\Delta\theta}\Big] \\ &+4(\bar{n}_Q\bar{n}_s)^{1/2}\text{Re}\Big[\Lambda_i\Gamma_i^* e^{-i\Delta\theta}\Big]\left(\bar{n}_Q|\Lambda_i|^2 + (2+\bar{n}_s)|\Gamma_i|^2\right) \\ &+4(\bar{n}_{th}+1)\left(|\Lambda_i|^2 - |\Gamma_i|^2 - 1\right)\left(\bar{n}_i|\Lambda_i|^2 + (1+\bar{n}_s)|\Gamma_i|^2\right) \\ &+8(\bar{n}_s\bar{n}_Q)(\bar{n}_{th}+1)\left(|\Lambda_i|^2 - |\Gamma_i|^2 - 1\right)\text{Re}\Big[\Lambda_i\Gamma_i^* e^{-i\Delta\theta}\Big] \\ &+(2+4\bar{n}_s+\bar{n}_s^2)|\Gamma_i|^4 + 2(\bar{n}_{th}+1)^2\left(|\Lambda_i|^2 - |\Gamma_i|^2 - 1\right)^2\Big)\end{aligned} \tag{26}$$

where $\bar{r}_i = r(\bar{\omega}_i)$, $\bar{t}_i = t(\bar{\omega}_i)$, $\Delta\theta = \theta_i + \theta_s - 2\theta_p$, $\Lambda_i \equiv \Lambda_i(L)$, $\Gamma_i \equiv \Gamma_i(L)$, and $\bar{n}_{th} \equiv n_{th}(\bar{\omega}_i - \omega_p)$. In (26), when $\bar{n}_Q \neq 0$ the relative phase $\Delta\theta$ stays at $\pi/2$, which means that the optical power flows from the pump to the classical signal and to the quantum channel [21], [34]. Note that the second momentum number operator $\langle :\hat{N}_1\hat{N}_2: \rangle$ given by (26) contains 81 different terms, of which according with the expectation values present in (10)-(13), 33 are not null.

If the idler wave is fully generated inside the fiber $\bar{n}_Q = 0$. If both $\bar{n}_Q$ and $\bar{n}_s$ are null the FWM process is spontaneous and according with (25) and (26) $g^{(2)}(0) = 2$, which is in-line with previous theoretical [19] and experimental results [10].

IV. Results

In this section, we present the results obtained for the evolution of $g^{(2)}(0)$ with the fiber input optical power, in two distinct cases. First, we assume that there is no quantum channel, λ_Q, at fiber input. Second we admit that idler photons generated by FWM are created at wavelength λ_Q. In this work, we are assuming a filter bandwidth of 100 GHz, and an optical fiber with the following parameters: $\gamma = 2\ \text{W}^{-1}/\text{km}$, zero-dispersion wavelength $\lambda_0 = 1550.92$ nm, third and fourth-order dispersion coefficients at zero-dispersion wavelength $\beta_3 = 0.1\ \text{ps}^3/\text{km}$ and $\beta_4 = 10^{-4}\ \text{ps}^{-4}/\text{km}$, respectively, and length $L = 2.5$ km [35].

A. Idler Wave Fully Generated Inside the Fiber

In a low power regime, the stimulated FWM process produces only a few photons in the idler field [36]. In this section we analyze the $g^{(2)}(0)$ function in that regime.

In Fig. 2, we present the evolution of the $g^{(2)}(0)$ function given by (18) with the fiber input power. In that figure, the pump wavelength coincides with the fiber zero-dispersion wavelength. In Fig. 2(a), we plot $g^{(2)}(0)$ as a function of the input signal power, whereas in Fig. 2(b) we plot the evolution of $g^{(2)}(0)$ with the input pump power. In both figures the idler wave is fully generated inside the fiber.

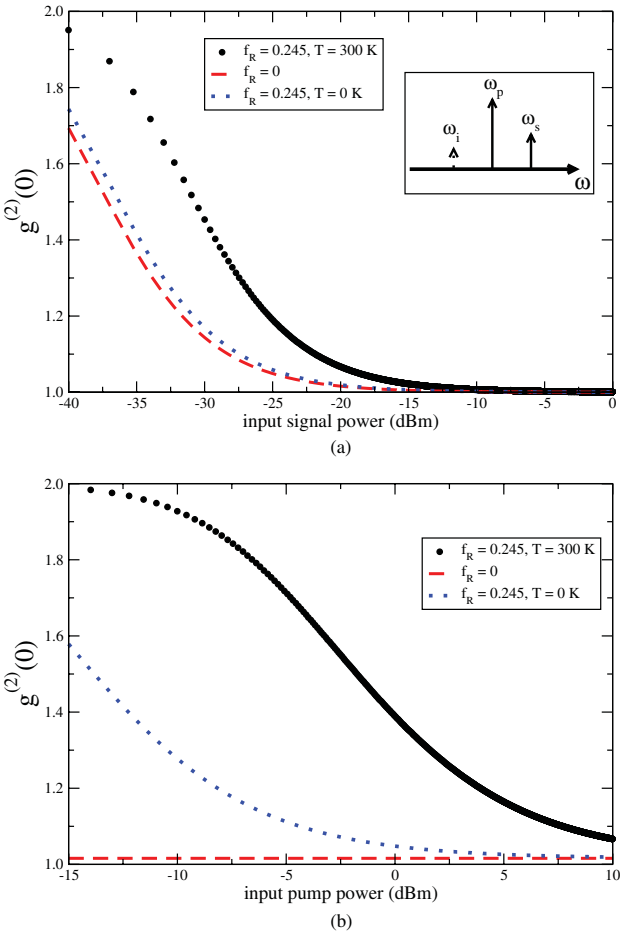

Fig. 2. Evolution of the $g^{(2)}(0)$ parameter with the fiber input power for the case of $P_Q = 0$ W (a) $P_p = 10$ dBm and (b) $P_s = -20$ dBm. The dots represent the case $f_R = 0.245$, the dashed lines represent $f_R = 0$, and the dotted lines represent the case $T = 0$ K. We have used $\lambda_p = \lambda_0$ and $\lambda_s = 1547.72$ nm. At fiber output the expected idler optical power is $P_Q < 0.4$ μW for (a), and $P_Q < 5$ nW for (b).

From Fig. 2(a) we can see that, the idler field is mostly described by a thermal statistics, when the input signal power is maintained at a low level. Increasing the signal power the statistics of the idler wave at fiber output evolves from thermal to Poissonian. After that, a continuous increase of the signal power does not change the statistics of the idler wave. The results plotted in Fig. 2(a) show that, the Raman scattering increases the variance of the photon distribution of the idler wave when compared with the limit $f_R = 0$. This increase leads a high value on the $g^{(2)}(0)$ function. Fig. 2(a) also shows that, at zero temperature the variance of the idler photons decrease when compared with the case $T = 300$ K. This arises from (11) where $n_{th}(\Omega)$ is null when $T = 0$ K.

It can be seen in Fig. 2(b) that, the statistics of the idler wave is very dependent on the Raman scattering process. In a low pump and signal power limit the dominant process inside the fiber is the spontaneous Raman scattering [19]. Due to that, the statistics of the idler wave remains approximately thermal over a high range of input pump power. This is also verified when $T = 0$ K, due to the fact that (11) is different from zero even at that temperature. This mean that at zero temperature the spontaneous Raman scattering continues to be a dominant process of creation of photons on the idler wave. When we ignore the Raman scattering process, $f_R = 0$, we observe that $g^{(2)}(0) \gtrsim 1$. This reveals the bunched nature of the photons generated by the FWM process.

B. Idler Photons Generated at λ_Q

In this section, we admit that at the fiber input there exist a coherent quantum channel, ω_Q, and idler photons, ω_i, will be created at ω_Q. The idler photons are generated inside the optical fiber through the combined processes of FWM and Raman scattering. The coherent quantum channel ω_Q at fiber input contains only a few photons in that frequency mode, and it is described by a Poissonian statistics, see Fig. 1. At fiber output the coherent quantum channel contains photons created by both FWM and Raman scattering processes. In that scenario, the FWM and Raman photons can be seen as noise sources with respect to the quantum channel [8]. Since that noise photons are generated at frequency ω_Q, they cannot be removed from the quantum channel by using spectral filters on the detection stage, they must be seen as in-band noise [2], [8], [9].

In Fig. 3, we plot the variation of $g^{(2)}(0)$ given by (18), with the fiber input power. In Fig. 3(a), we plot $g^{(2)}(0)$ as a function of the input signal power, whereas Fig. 3(b) and 3(c) show the evolution of $g^{(2)}(0)$ with the fiber input pump and quantum channel power, respectively.

From Fig. 3(a) we can see that, the quantum channel changes its own statistics, from a Poissonian distribution at fiber input to a thermal statistics at the fiber output, when the input signal power is maintained in a low level. This change on the statistics arises from the spontaneous photons generated through FWM and Raman processes inside the fiber. Increasing the signal power the statistics of the quantum channel rapidly tends to a Poissonian distribution at both fiber input/output. This reveals the single mode nature of the quantum channel. Results plotted in Fig. 3(a) show that, the Raman scattering process does not dramatically change the statistics of that field.

In Fig. 3(b), we plot the evolution of $g^{(2)}(0)$ with the input pump power. From Fig. 3(b) we can see that, for low pump power levels the second-order coherence function remains approximately constant, $g^{(2)}(0) \approx 1$ at fiber output. This is an expected result since in that pump power limit, the unique contribution for the generation of photons arises from the expectation value of the noise operator given by (11), which is a very small contribution when compared with the input fiber mean photon flux for the quantum channel field (24). However, an increase on the input pump power leads to a rapidly change on the statistics of the quantum channel, from a Poissonian, at fiber input, to a thermal at fiber output. This change is mainly due to spontaneous processes that occurs inside the optical fiber. Moreover, if we continue to increase the pump power the statistics at fiber output changes again from a thermal to Poissonian. This is due to the increase of the stimulated FWM process, in which the variance of the mean photon number is smaller when compared with the Raman scattering process. This happens because stimulated FWM is

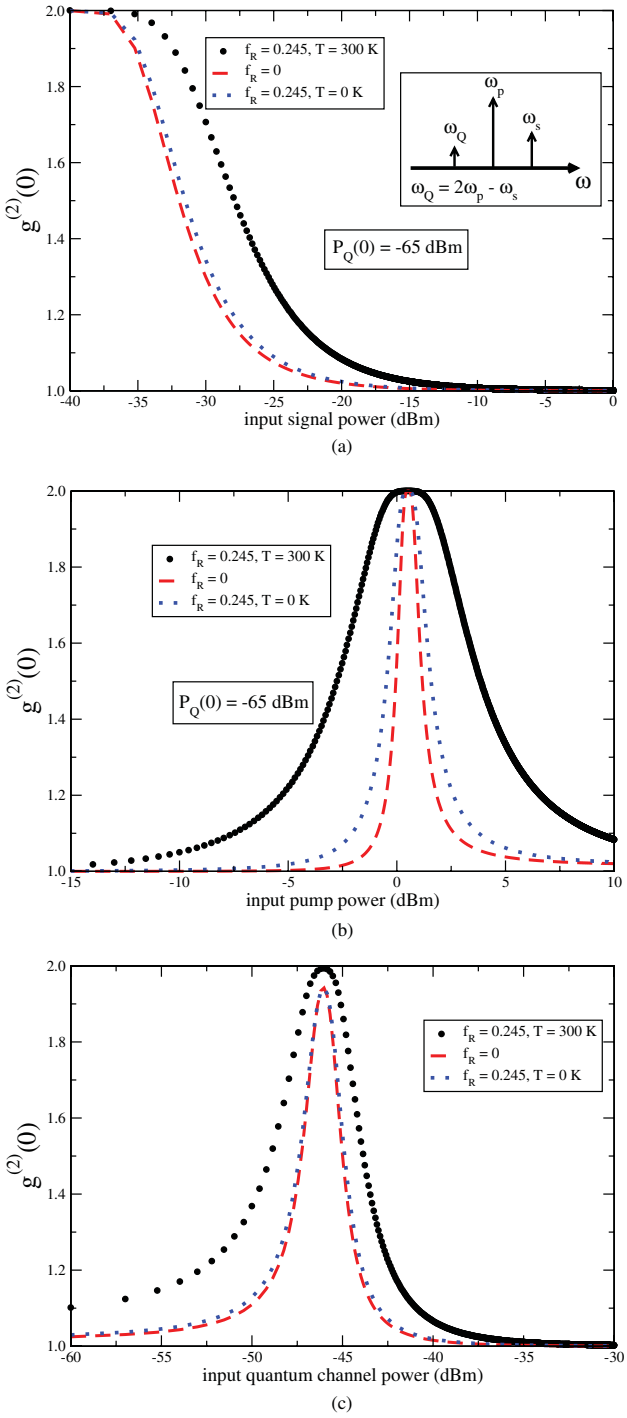

Fig. 3. Evolution of the $g^{(2)}(0)$ parameter with the fiber input power (a) $P_p = 10$ dBm and $P_Q = -65$ dBm, (b) $P_s = -20$ dBm and $P_Q = -65$ dBm, and (c) $P_p = 10$ dBm and $P_s = -20$ dBm. The dots represent the case $f_R = 0.245$, the dashed lines represent $f_R = 0$, and the dotted lines represent the case $T = 0$ K. We have used $\lambda_p = \lambda_0$ and $\lambda_s = 1547.72$ nm. At fiber output the expected idler optical power is $P_Q < 0.4$ μW for (a), $P_Q < 4$ nW for (b), and $P_Q < 0.2$ μW for (c).

almost a single frequency mode process. When we compare the cases $T = 0$ K with $T = 300$ K we see that the Raman noise given by (11) dominates the evolution of $g^{(2)}(0)$ with the input pump power.

In Fig. 3(c), we show the evolution of $g^{(2)}(0)$ as a function of the fiber input power of the quantum channel. From Fig. 3(c) we can see that, for low input power the statistics of the quantum channel remains approximately Poissonian at fiber input/output. However, an increase on the input power leads to a rapidly evolution of the statistics of that optical field, from Poissonian to thermal, revealing the spontaneous nature of FWM and Raman processes that occurs inside the fiber. For high power levels, the dominant process is the stimulated FWM, and the quantum channel evolves from a thermal statistics to a Poissonian. Since (11) does not depend on the input mean photon flux of the quantum channel the

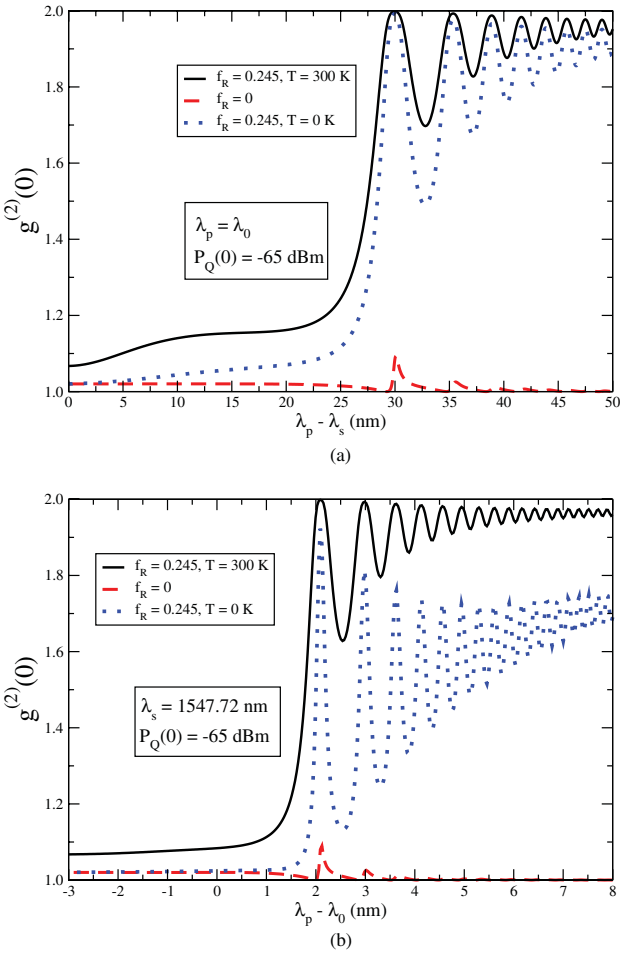

Fig. 4. Evolution of the $g^{(2)}(0)$ parameter with wavelength detuning. (a) Evolution of the $g^{(2)}(0)$ with the wavelength separation between pump and signal field. (b) $g^{(2)}(0)$ parameter as a function of $\lambda_p - \lambda_0$. At fiber output the expected idler optical power is $P_Q < 4$ nW for both (a) and (b).

Raman noise does not affect the statistics of that field. Results present in Fig. 3(c) show that the presence of the Raman scattering increase the variance of the quantum channel, when compared with the limit $f_R = 0$.

In Fig. 4, we plot $g^{(2)}(0)$, given by (18), as a function of wavelength detuning between pump and signal fields, Fig. 4(a), and between pump and fiber zero-dispersion wavelength, Fig. 4(b).

It can be seen in Fig. 4(a) and in Fig. 4(b) that, $g^{(2)}(0)$ tends to a thermal distribution at fiber output with the increase of the wavelength detuning. This happens because the frequency of the quantum channel approaches the maximum Raman gain. For small values of wavelength detuning the $g^{(2)}(0)$ function is slightly higher than one in both Fig. 4(a) and Fig. 4(b). This is due to photons generated on the quantum channel through the Raman scattering process inside the fiber. This can be seen in Fig. 4 when we compared the case $f_R = 0.245$ with $f_R = 0$. It can also be seen in Fig. 4(a) that, the Raman noise given by (11) does not change significantly the evolution of $g^{(2)}(0)$ with $\lambda_p - \lambda_s$. Otherwise, in Fig. 4(b) at zero temperature the value of $g^{(2)}(0)$ is smaller when compared with $T = 300$ K. This is due to the phase-matching condition given by (6) which takes a small value in the case presented in Fig. 4(a) than in Fig 4(b), due to the fact that $\lambda_p = \lambda_0$ in Fig. 4(a). This leads to a high generation of photons through stimulated FWM process, instead of Raman scattered photons.

V. Conclusion

In summary, we show that the statistics of the idler wave generated through FWM follows a thermal distribution when the fiber input power is maintained in a low level. This arises from the thermal nature of the photons generated through spontaneous FWM and through Raman scattering inside the fiber. That happens because those nonlinear processes create photons in several different frequency modes (large frequency bandwidth) with short coherence time. However, an increase on the input power rapidly leads to a Poissonian distribution for the idler photons, at the fiber output. This change on the statistics happens when the stimulated FWM becomes the dominant process, and the photons are created at a single frequency mode, ω_i. Our results also show that the in-band noise photons created by FWM and Raman scattering processes can change the statistics of a quantum channel used for QKD. At low power level the statistics of the coherent quantum channel can evolve from Poissonian to thermal. Our findings also show that when we increase the wavelength detuning between the pump and signal the coherent quantum channel evolves from a Poissonian statistics to a thermal one. This is due to the fact that the quantum channel approaches the maximum Raman gain. In addition, we have shown that for small wavelength detunings between pump and signal fields the impact of the Raman scattering on the quantum channel is almost negligible, and the statistics of that channel remains the same through propagation.

References

[1] N. Gisin, G. Ribordy, W. Tittel, and H. Zbinden, "Quantum cryptography," *Rev. Mod. Phys.*, vol. 74, no. 1, pp. 145–195, 2002.

[2] P. Eraerds, N. Walenta, M. Legré, N. Gisin, and H. Zbinden, "Quantum key distribution and 1Gbps data encryption over a single fibre," *New J. Phys.*, vol. 12, no. 6, pp. 063027-1–063027-9, 2010.

[3] P. Townsend, "Simultaneous quantum cryptographic key distribution and conventional data transmission over installed fibre using wavelength-division multiplexing," *Electron. Lett.*, vol. 33, no. 3, pp. 188–190, 1997.

[4] G. Agrawal, *Lightwave Technology: Telecommunication Systems*. New York: Wiley, 2005.

[5] N. Muga, M. Ferreira, and A. Pinto, "QBER estimation in QKD systems with polarization encoding," *J. Lightw. Technol.*, vol. 29, no. 3, pp. 355–361, 2011.

[6] T. Xia, D. Chen, G. Wellbrock, A. Zavriyev, A. Beal, and K. Lee, "In-band quantum key distribution QKD on fiber populated by high-speed classical data channels," in *Proc. Opt. Fiber Commun. Conf. Nat. Fiber Opt. Eng.*, Mar. 2006, pp. 1–3.

[7] N. Silva, N. Muga, and A. Pinto, "Influence of the stimulated Raman scattering on the four-wave mixing process in birefringent fibers," *J. Lightw. Technol.*, vol. 27, no. 22, pp. 4979–4988, 2009.

[8] N. A. Peters, P. Toliver, T. E. Chapuran, R. J. Runser, S. R. McNown, C. G. Peterson, D. Rosenberg, N. Dallmann, R. J. Hughes, K. P. McCabe, J. E. Nordholt, and K. T. Tyagi, "Dense wavelength multiplexing of 1550 nm QKD with strong classical channels in reconfigurable networking environments," *New J. Phys.*, vol. 11, no. 4, pp. 045012-1–045012-16, 2009.

[9] B. Qi, W. Zhu, L. Qian, and H.-K. Lo, "Feasibility of quantum key distribution through a dense wavelength division multiplexing network," *New J. Phys.*, vol. 12, no. 10, pp. 103042-1–103042-18, 2010.

[10] P. L. Voss, R. Tang, and P. Kumar, "Measurement of the photon statistics and the noise figure of a fiber-optic parametric amplifier," *Opt. Lett.*, vol. 28, no. 7, pp. 549–551, 2003.

[11] G. Zambra, M. Bondani, A. S. Spinelli, F. Paleari, and A. Andreoni, "Counting photoelectrons in the response of a photomultiplier tube to single picosecond light pulses," *Rev. Scient. Instrum.*, vol. 75, no. 8, pp. 2762–2765, 2004.
[12] G. Zambra, A. Andreoni, M. Bondani, M. Gramegna, M. Genovese, G. Brida, A. Rossi, and M. G. A. Paris, "Experimental reconstruction of photon statistics without photon counting," *Phys. Rev. Lett.*, vol. 95, no. 6, pp. 063602-1–063602-4, 2005.
[13] R. Loudon, *The Quantum Theory of Light*, 3rd ed. New York: Oxford Univ. Press, 2000.
[14] M. Beck, "Comparing measurements of $g^{(2)}(0)$ performed with different coincidence detection techniques," *J. Opt. Soc. Amer. B*, vol. 24, no. 12, pp. 2972–2978, 2007.
[15] E. A. Goldschmidt, M. D. Eisaman, J. Fan, S. V. Polyakov, and A. Migdall, "Spectrally bright and broad fiber-based heralded single-photon source," *Phys. Rev. A*, vol. 78, no. 1, pp. 013844-1–013844-4, 2008.
[16] H. J. McGuinness, M. G. Raymer, C. J. McKinstrie, and S. Radic, "Quantum frequency translation of single-photon states in a photonic crystal fiber," *Phys. Rev. Lett.*, vol. 105, no. 9, pp. 093604-1–093604-5, 2010.
[17] J. A. Slater, J.-S. Corbeil, S. Virally, F. Bussières, A. Kudlinski, G. Bouwmans, S. Lacroix, N. Godbout, and W. Tittel, "Microstructured fiber source of photon pairs at widely separated wavelengths," *Opt. Lett.*, vol. 35, no. 4, pp. 499–501, 2010.
[18] D. de Brito and R. Ramos, "Analysis of heralded single-photon source using four-wave mixing in optical fibers via wigner function and its use in quantum key distribution," *IEEE J. Quantum Electron.*, vol. 46, no. 5, pp. 721–727, May 2010.
[19] Q. Lin, F. Yaman, and G. P. Agrawal, "Photon-pair generation in optical fibers through four-wave mixing: Role of Raman scattering and pump polarization," *Phys. Rev. A*, vol. 75, no. 2, pp. 1–20, 2007.
[20] E. Brainis, "Four-photon scattering in birefringent fibers," *Phys. Rev. A*, vol. 79, no. 2, pp. 023840-1–023840-14, 2009.
[21] G. Agrawal, *Nonlinear Fiber Optics*, 3rd ed. New York: Academic, 2001.
[22] R. W. Hellwarth, *Third-Order Optical Susceptibilities of Liquids and Solids*. New York: Oxford Univ. Press, 1977.
[23] Q. Lin and G. P. Agrawal, "Raman response function for silica fibers," *Opt. Lett.*, vol. 31, no. 21, pp. 3086–3088, 2006.
[24] N. A. Silva, N. J. Muga, and A. N. Pinto, "Evolution of first-order sidebands from multiple FWM processes in HiBi optical fibers," *Opt. Commun.*, vol. 284, no. 13, pp. 3408–3415, 2011.
[25] M. Artoni and R. Loudon, "Propagation of nonclassical light through an absorbing and dispersive slab," *Phys. Rev. A*, vol. 59, no. 3, pp. 2279–2290, 1999.
[26] M. Fox, *Quantum Optics: An Introduction*. New York: Oxford Univ. Press, 2006.
[27] K. J. Blow, R. Loudon, S. J. D. Phoenix, and T. J. Shepherd, "Continuum fields in quantum optics," *Phys. Rev. A*, vol. 42, no. 7, pp. 4102–4114, 1990.
[28] S. Barnett and P. Radmore, *Methods in Theoretical Quantum Optics*. New York: Oxford Univ. Press, 2002.
[29] R. Chiao and J. Garrison, *Quantum Optics*. New York: Oxford Univ. Press, 2008.
[30] W. H. Louisell, A. Yariv, and A. E. Siegman, "Quantum fluctuations and noise in parametric processes. I," *Phys. Rev.*, vol. 124, no. 6, pp. 1646–1654, 1961.
[31] S. M. Barnett, J. Jeffers, A. Gatti, and R. Loudon, "Quantum optics of lossy beam splitters," *Phys. Rev. A*, vol. 57, no. 3, pp. 2134–2145, 1998.
[32] G. Li, T. C. Zhang, Y. Li, and J. M. Wang, "Photon statistics of light fields based on single-photon-counting modules," *Phys. Rev. A*, vol. 71, no. 2, pp. 023807-1–023807-6, 2005.
[33] G. Li, T. Zhang, Y. Li, and J. Wang, "Correction of photon statistics of quantum states in single-photon detection," *Quantum Opt. Applicat. Comput. Commun. II*, vol. 134, pp. 134–142, Nov. 2005.
[34] K. Inoue and T. Mukai, "Signal wavelength dependence of gain saturation in a fiber optical parametric amplifier," *Opt. Lett.*, vol. 26, no. 1, pp. 10–12, 2001.
[35] B. P. Pal, *Guided Wave Optical Components and Devices*. San Diego, CA: Academic, 2005.
[36] N. A. Silva, N. J. Muga, and A. N. Pinto, "Effective nonlinear parameter measurement using FWM in optical fibers in a low power regime," *IEEE J. Quantum Electron.*, vol. 46, no. 3, pp. 285–291, Mar. 2010.

Nuno A. Silva was born in Fafe, Portugal, in 1981. He received the degree in physics from the University of Minho, Portugal, and the M.S. degree in physics from the University of Aveiro, Aveiro, Portugal, in 2006 and 2008, respectively. He is currently pursuing the Ph.D. degree with the University of Aveiro.

He joined the Institute of Telecommunications, Aveiro, in 2007, where he is currently a Researcher with the Optics Communications Group. His current research interests include nonlinear fiber optics, polarization, and quantum effects in optical fibers.

Álvaro J. Almeida was born in Portugal, in 1984. He received the Degree in physics and the M.Sc. degree in physics from the University of Aveiro, Aveiro, Portugal, in 2007 and 2008, respectively.

He is currently a Researcher with the Optics Communications Group, Institute of Telecommunications, Aveiro. His current research interests include generation, transmission, and detection of single and entangled photons, for quantum key distribution systems.

Armando Nolasco Pinto (M'99–SM'07) graduated in electronic and telecommunications engineering and received the Ph.D. degree in electrical engineering from the University of Aveiro, Aveiro, Portugal, in 1994 and 1999, respectively.

He was an Assistant Professor with the Electrical, Telecommunications and Informatics Department, University of Aveiro, and a Researcher with the Institute of Telecommunications, in 2000. He was a Visiting Professor with the Institute of Optics, University of Rochester, Rochester, NY, from 2006 to 2007. Currently, he leads a research group with the Institute of Telecommunications, focusing on high-speed optical communication systems and networks. He has published more than 100 scientific papers in international journals and conferences.

Dr. Pinto has served on the technical committees of various international scientific conferences. He is currently an Editorial Board Member of the *International Journal of Optics*, and a member of the Optical Society of America.